npj Heritage Science

https://doi.org/10.1038/s40494-026-02753-8

Article in Press

Multi-analytical investigations of earthen wall paintings from the *Templo Pintado*: stratigraphy and material characterisation for conservation assessment

Received: 12 December 2025

Accepted: 14 June 2026

Cite this article as: Cappai, M., Pia, G., Pozzi-Escot, D. *et al.* Multi-analytical investigations of earthen wall paintings from the *Templo Pintado*: stratigraphy and material characterisation for conservation assessment. *npj Herit. Sci.* (2026). https://doi.org/10.1038/s40494-026-02753-8

Marta Cappai, Giorgio Pia, Denise Pozzi-Escot, Gianella Pacheco Neyra, Stefania Porcu & Daniele Chiriu

Multi-analytical investigations of earthen wall paintings from the *Templo Pintado*: stratigraphy and material characterization for conservation assessment

Marta Cappai[1], Giorgio Pia[1], Denise Pozzi-Escot[3], Gianella Pacheco Neyra[4], Stefania Porcu[2,*] and Daniele Chiriu[2]

[1] Department of Mechanical, Chemical, and Materials Engineering, University of Cagliari, Via Marengo 2, 09123 Cagliari, Italy

[2] Department of Physics, University of Cagliari, SP8, 09042 Monserrato (CA), Italy

[3] Museo Pachacamac, Antigua Carretera Panamericana Sur Km. 31.5, Distrito de Lurín, Lima, Peru

[4] Universidad Nacional Mayor de San Marcos, Av. Universitaria cruce con Av. Venezuela cuadra 34, Lima, Peru.

*corresponding author: stefania.porcu@dsf.unica.it

Abstract

Earthen wall paintings present complex multilayer structures susceptible to long-term physicochemical deterioration. This study presents a multi-analytical characterization (optical microscopy, XRD, Raman spectroscopy, SEM-EDS) of previously uncharacterized fragments from Sector 3 of the Templo Pintado (Pachacamac, Peru) extending the analytical coverage of the site and assessing the continuity of material and technological features across the monument, while re-examining the long-standing hypothesis of organic binders. The results reveal jarosite-based yellow pigments, hematite-rich reds, and silicate-carbonate plasters containing illitic and chloritic phases, with evidence of multiple repainting phases. Weak but consistent Raman signals in the 1200–1700 cm^{-1} range indicate the presence of organic compounds, possibly of plant-based or resinous origin, although their definitive assignation as original binding materials is limited by the analytical methodology employed. The detection of anatase suggests later conservation interventions. Overall, the dataset provides a reference framework for distinguishing original materials from subsequent additions and supports conservation assessment.

Keywords: Templo Pintado; Pachacamac; Mural painting; Pigments; Conservation; Raman Spectroscopy.

Introduction

Historic buildings can be interpreted as stratified material systems resulting from cumulative human interventions over time where modifications, additions, replacements, and restorations are preserved as superimposed layers and microlayers, recording both material history and cultural development [1–4].

In the specific case of wall paintings executed on earthen plasters, this stratification often results in highly heterogeneous and fragile multilayer systems [5], in which mineral pigments, inorganic binders, clays, carbonates, and occasionally organic additives form complex assemblages [6–8] undergoing long-term physical and chemical transformation [9,10].

Earthen substrates are particularly vulnerable due to high porosity, hygroscopic behaviour, and low mechanical cohesion, making them highly sensitive to environmental stressors such as humidity fluctuations, soluble salts, and capillary action, which accelerate deterioration [11–15]. Although surfaces may appear macroscopically uniform, they often conceal complex stratigraphic architectures that require integrated analytical approaches to be resolved [1,16]. Multi-analytical methods, including Raman spectroscopy, scanning electron microscopy, X-ray diffraction, and cross-sectional microscopy, are essential to distinguish original layers from later interventions and to identify alteration products [5,17–21].

At the same time, the compositional characterisation of the paint layers, including the potential presence of organic components, is relevant not only from an interpretative perspective but also from a conservation standpoint [6,22–25]. The identification of possible organic binders represents, in fact, critical information for the planning of future conservation interventions, as their presence requires particular caution in the use of solvents or treatments that could lead to dissolution or alteration of these components [26,27]. Moreover, such information provides a basis for technological coherence in the evaluation of modern protective materials, enabling a discussion of continuity or compatibility between ancient painting practices and contemporary conservation approaches [23,24,28].

In this methodological and material framework, the *Templo Pintado* of Pachacamac represents a particularly critical and informative case study. The *Templo Pintado* is one of the most emblematic structures of the Archaeological Sanctuary of Pachacamac, a major religious center on the central Peruvian coast (Fig. 1a and b) occupied for over a millennium [29]. The site is situated on an irregular plain dominated by four rocky promontories and bordered by diverse ecosystems [29]. The climate of the area can be classified as hot desert climate (BWh) according to the Köppen-Geiger classification [30–32]. Human occupation at Pachacamac dates back to the Archaic period, but the sanctuary was first built by the Lima culture (200-600 CE), expanded during the Wari period (600-1100 CE), and reached its greatest religious prominence under the Ychsma (1100-1470 CE) [33–35]. After its incorporation into the Inca Empire around 1470 CE, the sanctuary remained an important ceremonial center until the Spanish conquest in 1533, when the oracle was destroyed and the complex progressively abandoned [33,34,36,37]. The *Templo Pintado* is a trapezoidal, stepped adobe structure set on a low rocky promontory, with fragments of polychrome wall paintings concentrated mainly along its North Front (Fig. 1c) [29,33,38,39].

The paintings were executed using the technique known as *temple mate*, in which finely ground mineral pigments were mixed with water and applied to the earthen plaster surface using cotton wads and hair-based brushes [38]. The decorative programme is organised into three main pictorial phases, identified through the combined analysis of stratigraphic superposition, macroscopic observation, and iconographic comparison [29]. The first phase is characterised by human and animal figures outlined in black and painted in yellow ochre, white, and green on a garnet red background; subsequent phases (second and third) introduced wide alternating bands of vermilion red and pale yellow, with figurative elements rendered in contrasting colours and occasional green-grey tones [29,40]. The chromatic terminology adopted in the literature, including designations such as “vermilion red” and “pale yellow”, reflects the historical nomenclature established by early analytical studies of the site and denotes chromatic categories rather than mineralogical identifications [29,38]. The susceptibility of earthen materials to weathering necessitated repeated maintenance interventions during each phase, ranging from simple repainting to full plaster replacement, producing complex sequences of superimposed layers [38,41].

Over time, different studies and observations have provided valuable information on selected materials, stratigraphic features, and conservation conditions of the *Templo Pintado* wall paintings

[29,38,40–47]. Taken together, these investigations reflect the diversity of analytical approaches, research objectives, and historical contexts in which the site has been studied, while also highlighting the heterogeneous and fragmentary nature of the available data. A detailed review of these studies is provided in Supplementary Information S1.

Among the issues that have emerged from this body of literature, one concerns the possible presence of organic components in the painting technology. Some of the earliest analytical works proposed the use of a natural organic binder on the basis of experimental observations and technological analogies [38]. However, subsequent investigations, employing different analytical strategies and often focusing primarily on mineralogical characterization, have not provided a clear instrumental confirmation of this hypothesis [29,44,45]. As a result, the question of organic components in the pictorial layers remains unresolved and represents one of the open issues persisting in the archaeometric study of the *Templo Pintado* wall paintings, with potential implications for both technological interpretation and conservation practice.

The present study was designed to advance knowledge on the Templo Pintado wall paintings on multiple, interconnected fronts. First, it extends the analytical coverage of the site to Sector 3 of the North Front, an area not previously subjected to material characterization, thereby contributing to a more complete picture of the technological practices employed across the monument and providing a diagnostic baseline for conservation planning specific to this sector. Second, the analytical strategy integrates optical microscopy, XRD, Raman spectroscopy, and SEM-EDS on the same set of samples, combining methods that in previous investigations of the Templo Pintado had been applied separately, thus enabling cross-validation among complementary methods. Third, Raman spectroscopy was deployed not exclusively for mineralogical identification but specifically as a tool to probe for signals compatible with organic residues, with the explicit aim of re-examining the long-standing hypothesis of organic binders in the painting technology [38], a hypothesis that had remained unconfirmed in all subsequent instrumental investigations and carries direct implications for conservation practice.

Given the consistent analytical data documented for other sectors of the North Front in previous investigations [29,38,44–47], the study was also designed to evaluate whether the same technological framework extends to Sector 3. Confirming this expected continuity is nonetheless informative: it demonstrates that standardized material choices and preparation practices operated systematically

across the entire monument, providing a scientifically grounded basis for coordinated conservation planning and strengthening the validity of previous diagnostic data as a reference framework.

On this basis, the present study is structured around an integrated evaluation of stratigraphic organisation, combining cross-sectional optical microscopy on a representative sample with direct Raman and SEM-EDS investigation of exposed inner layers, pigment composition, and microstructural features of the analysed fragments, with the aim of interpreting the technological choices underlying the wall paintings, resolving long-standing open questions regarding material composition, and providing a scientifically grounded framework for future conservation interventions.

Methods

Archaeological samples

Ten painted plaster fragments (TP_1, TP_4, TP_6, TP_8, TP_9, TP_12, TP_A, TP_B, TP_C, and TP_D) were collected in situ during excavation and surface cleaning activities carried out in North Front, Sector 3, terrace level 9, of the *Templo Pintado* (Fig. 2a), a sector that, to the best of our knowledge, has not been previously subjected to material characterisation analyses in the literature. No samples were removed from painted surfaces still in place on the structure. All fragments analyzed in the present study were already detached from the masonry at the time of collection and originated from collapse deposits accumulated on the stepped architectural elements of the structure. During cleaning operations, loose and incoherent deposits were carefully removed using soft brushes and low-pressure manual air blowing. Painted plaster portions still adhering to the masonry were consolidated in situ. Painted plaster fragments recovered from the debris and not suitable for repositioning onto the original surfaces were selected for analysis. Among the numerous fragments recovered during these operations, those exhibiting a better state of preservation and integrity were preferentially selected in order to ensure the reliability of the analytical results. Loose surface deposits related to burial conditions were removed by gentle dry mechanical cleaning using a handheld air blower. The samples were catalogued, wrapped in Japanese paper, placed in plastic containers, and transported to the laboratory, where they were

kept under controlled temperature and relative humidity conditions (T = 23 ± 2 °C; RH = 55 ± 5%) prior to analysis.

On the surface layer, the samples exhibit the two most frequently observed colors in the decorative surfaces of the *Templo Pintado*: pale yellow and vermilion red, both characteristic to the second and third pictorial phases [29], where "vermilion red" follows the historical terminology adopted in previous studies and denotes a chromatic designation rather than a mineralogical identification such as mercury sulfide. Additionally, among the stratifications, colors associated with the first pictorial phase, such as yellow ochre, are clearly visible.

The samples can therefore be divided into two groups based on their surface color: pale yellow group (TP_1, TP_4, TP_6, TP_8, TP_9 and TP_12) and the vermilion red group (TP_A, TP_B, TP_C and TP_D). Given the similarity among samples of the same superficial color, one representative sample from each group will be described (TP_6 for the pale yellow group and TP_B for the vermilion red group). Descriptions of the remaining samples are provided in the Supplementary Information S2 - S9. This classification reflects the macroscopic appearance of the fragments and is adopted for descriptive purposes, without restricting the analytical investigation to these surface layers.

In general, the pale yellow samples are characterised by a markedly powdery and highly degraded pictorial surface, while the vermilion red samples display a relatively higher cohesion of the paint layers, showing limited powdering but a greater tendency towards exfoliation, with detachment occurring as thin flakes. In all cases, the plaster substrate appears friable and structurally compromised, resulting in minor particle loss during sample handling.

While surface characterization was conducted on the full set of samples, the investigation of internal stratigraphic layers was carried out on fragments exhibiting the most complete and preserved sequences: fragment TP_C was selected for cross-sectional optical microscopy, as it showed the best state of preservation allowing reliable preparation of a polished section, while fragment TP_B was investigated by Raman spectroscopy and SEM-EDS directly on the as-received fragment, accessing the inner strata naturally exposed along its lateral edges.

In Fig. 2b-d is reported the sample named TP_6. A schematic representation of the macroscopically observed stratigraphy is provided in Fig. 2e. Two superficial painted layers are observed in the sample: an outer pale yellow layer (Fig. 2b) and an inner yellow ochre layer in

contact with the plaster (Fig. 2c). The yellow ochre became visible following the removal of the pale yellow layer, which was carried out to obtain a small amount of powder for XRD analysis. In the section view, the painting appears to have been applied on a regularizing plaster layer of approximately 3 mm. Beneath this, a further red painted layer (~0.7 mm thick) is visible, laid on a plaster that in some areas thins out until it disappears, bringing the red paint layer into direct contact with the two outer layers. The pale yellow surface is highly pulverized. The clast size within the earth mortar does not exceed 1 mm. The earth-based plaster appears to be highly porous, with macroscopic voids ranging from 1 to 2 mm, likely related to the plaster application process and the nature of the granular earthen mortar. The presence of macroscopic voids is often attributed to air bubbles entrapped during the manual mixing process and to the difficulty in fully compacting stiff, low-moisture mortars, which are frequently employed to minimize drying shrinkage [48,49]. Furthermore, variations in the void ratio can result from production defects inherent to the granular nature of the material and specific application practices, such as the re-tempering of the mortar with water to maintain workability during application [48–50].

Descriptions of the other samples with a pale yellow surface (TP_1, TP_4, TP_8, TP_9 and TP_12) are included in Supplementary Information S2 - S6.

In Fig. 2f-g is reported the sample named TP_B. A schematic representation of the macroscopically observed stratigraphy is provided in Fig. 2h. This sample is a fragment of painted earthen plaster bearing vermilion, green–grey, and black pigments on the surface. It is multilayered, and macroscopically four alternating vermilion red and pale yellow layers were observed in the surface. The green-grey and black areas form part of a decorative design applied above the outermost vermilion layer. The total thickness of the four surface painted layers reaches approximately 1.2 mm in the thickest sections. The surface layer appears compact and still retains visible marks from the layer application. Although generally flat and regular, a slight roughness is present due to aeolian corrasion. Below the surface layers, the sample has the following stratigraphy: a layer of plaster approximately 5 mm thick, followed by a layer of vermilion paint layer 0.6 mm thick, then another layer of plaster 3 mm thick, followed by a layer of yellow ochre paint and a layer of garnet red paint, and finally a layer of plaster 6 mm thick. Traces of red are also visible on the back of the fragment, suggesting that the sample was probably part of a thicker

plaster structure with additional layers. No macroscopic differences were observed between the various layers of mortar. The size of the clasts does not exceed 1 mm.

Descriptions of the other samples with a vermilion red surface (TP_A, TP_C and TP_D) are included in Supplementary Information S7 - S9.

The stratigraphic variability macroscopically observed and described between the pale yellow and vermilion red samples from Sector 3 is consistent with a model of active, localised maintenance within each pictorial phase. The distinction between the three phases reflects documented iconographic and material choices [29,40–42], but each phase appears to have been sustained through episodic, localised interventions: in some areas, repainting was applied directly onto the pre-existing paint layer, while in others it was preceded by the application of a new preparatory plaster layer. This type of localised intervention naturally generates a heterogeneous stratigraphic record, with simple and complex sequences coexisting within the same sector, as documented by the comparison between samples TP_6 and TP_B described above and those reported in Supplementary Information (S2 - S9).

Characterization Techniques

The samples under investigation were subjected to a range of diagnostic techniques to assess their morphological and compositional characteristics.

Surface and cross-sectional observations were carried out using reflected light optical microscopy with a Carl Zeiss Axioscop 40 light microscope. Surface observations were performed on all samples, while cross-sectional ones were carried out on a single representative sample (TP_C, described in Supplementary Information S8), belonging to the vermilion red sample group. For cross-sectional optical microscopy, sample TP_C was embedded in epoxy resin, sectioned, and the exposed surface was progressively polished to obtain a flat and readable cross-section. Only one sample was prepared as a cross-section, given the overall similarity among the samples and to minimize invasive interventions on the archaeological material. Observations were performed at various magnifications (2.5×, 5× and 10×) to highlight morphological features at different scales.

The XRD investigation was conducted on the outermost paint layers (pale yellow and vermilion red) and the plaster of all ten collected fragments. This limitation to surface layers was due to the extreme mechanical fragility of the samples, which prevented the mechanical isolation of inner paint layers without causing fragmentation and mixing of material from adjacent layers. The surface layers were carefully detached using a stainless-steel scalpel and subsequently finely ground in an agate mortar to obtain a homogeneous powder for analysis. Mineralogical composition was then investigated by XRD using a Bruker D8 Advance diffractometer equipped with a multi-mode LYNXEYE XE-T detector and Cu Kα radiation (λ = 1.5406 Å). Data were acquired in Bragg-Brentano geometry over a 2θ angular range of 3°-90° for crystalline phase identification. The resulting diffractograms were processed and interpreted using the MAUD software.

Raman spectroscopy and SEM-EDS were used to investigate the mineralogical and elemental composition of the painted fragments. Access to the underlying layers was achieved by analyzing the exposed stratigraphic sections along the lateral edges of the fragments. In selected cases, minimal mechanical cleaning (removal of ~0.5-1 mm of loose material) was performed to obtain a clean analytical surface, allowing direct Raman and SEM-EDS measurements on inner paint layers without sampling cross-sections. Loose debris were then removed by gentle dry cleaning using low-pressure manual air blowing. Analyses were subsequently performed directly on the fragment, on both the painted surface and the exposed inner layers. Results are reported for sample TP_B, which due to its complex multi-layer stratigraphy provided access to all the main pigment types identified across the sample set. Near-infrared micro-Raman scattering measurements were performed in back-scattering geometry using the 1064 nm line of a Nd-YAG laser. The analyses were conducted with a B&WTEK (Newark, NJ, USA) i-Raman Ex compact spectrometer, providing a spectral resolution of 8 cm^{-1}. For each configuration, spectra were acquired with an integration time of approximately 60 s (five replicas) and with a laser power between 5 and 10 mW, focused onto a 0.3 mm^2 spot through a Raman Video MicroSampling System equipped with a 20× Olympus objective for area selection. Each measurement area represents a sampling surface of about 1 cm^2. The samples were positioned to ensure that the painted surface was perpendicular to the incident laser beam.

SEM-EDS observations were performed using an FEI Quanta 200 ESEM operating in low-vacuum mode. Elemental data were acquired with a Thermo Scientific UltraDry INTX-10P-A detector managed through the Pathfinder software. For each analytical spot, spectra were recorded at 20 kV accelerating voltage with a live acquisition time of approximately 30 seconds. The samples were mounted on aluminum stubs and positioned to keep the investigated surface perpendicular to the electron beam during analysis. No conductive coating was applied.

Results and Discussion

Optical microscopy (MO)

The surfaces of the samples with yellow paint were observed at 2.5× and 5× magnifications. No substantial differences were noted among the surfaces of the various samples; all exhibited rather irregular morphologies. The pigment grains appeared poorly cohesive, both among themselves and with the underlying substrate, and the surfaces were characterized by evident pigment powdering phenomena (Fig. 3a). As a consequence of this pronounced surface irregularity and loss of cohesion, a uniform focus across the entire field of view could not be achieved, resulting in the locally reduced sharpness observed in Fig. 3a.

In sample TP_6 shown in Fig. 3b, the degraded pale-yellow surface exposes a yellow ochre layer that likely belongs to one of the earliest decorative phases of the *Templo*. Within this fragment, several fibrous elements are visible inside the pictorial layer. Since these fibers were detected only in this specific sample and could not be analytically characterized, they cannot be attributed to a deliberate additive nor to a systematic painting technique. However, their presence is consistent with documented cases of tool-derived residues in pre-Hispanic mural paintings. At Pachacamac, Muelle and Wells (1939) reported both cotton pads impregnated with pigments and hair fibers trapped within the painted layers, reflecting the use of cotton wads and hair-based brushes [38]. Likewise, Wright (2009) identified camelid hairs embedded in the pictorial layers of the Moche murals at Huaca de la Luna, demonstrating the incidental incorporation of brush bristles during paint application [51]. In this light, the fibers observed in our sample are best interpreted as accidental inclusions originating from the painting implements rather than functional constituents of the pigment mixture. The pigment particle size is generally below 10 μm, indicating a high

degree of grinding and refinement. In contrast, the protruding quartz grains from the preparatory plaster layer, now exposed due to the advanced state of pigment powdering, reach sizes of approximately 150 μm. This level of microscopic resolution provides crucial evidence on the sequence of surface preparations and pigment applications, offering insights that were previously inaccessible in studies based solely on macroscopic observations.

The surfaces of the vermilion red samples (TP_A, TP_B, TP_C and TP_D) appear more cohesive than those of the pale-yellow layers and do not show significant surface powdering. Instead, only localized damage, mainly attributable to wind erosion, is observed. Brushstroke marks from the original application technique are still clearly visible (Fig. 4a). At 5× magnification (e.g., Fig. 4b), pigment grains in the red layers also appear finely ground, with dimensions below 10 μm, again highlighting a high degree of mechanical processing of the pigment materials. Additionally, larger particles, ranging between 30 and 50 μm, can be distinguished. Cross-sectional observations (Fig. 4c-d-e) confirm that these grains are embedded within the paint layer itself rather than being restricted to the surface or derived from the underlying plaster. Their presence suggests that the pigment was mixed with a fine fraction, likely to improve the mechanical stability and workability of the paint layer.

The cross-section of sample TP_C (Fig. 4c-e) macroscopically reveals a complex stratigraphic sequence comprising alternating pictorial layers and plaster strata. From top to bottom, an uppermost painted portion of approximately 3 mm is identified, followed by a second plaster layer (7–9 mm), a first pictorial level of variable thickness (2–6 mm), and finally a basal plaster layer approximately 1 cm thick. The individual pictorial layers show variable thicknesses and, in some cases, do not extend continuously across the full surface of the stratum, suggesting the likely presence of figurative elements. The uppermost painted portion (Fig. 4e) comprises approximately 10 superimposed layers of predominantly vermilion red colour, within which a green layer and a pale yellow layer are also distinguished, compatible with both the second and third pictorial phases of the Templo Pintado, which present the same material composition. The differentiation between the second and third pictorial phases cannot be established on stratigraphic or compositional grounds alone, as it relies on the identification of iconographic diagnostic elements, which are not discernible on the small examined fragments. The underlying first pictorial level (Fig. 4d) consists of a succession of superimposed layers: a garnet red layer, followed by a thin yellow ochre layer,

a further garnet red layer, and finally a black layer, consistent with the chromatic characteristics documented for the first pictorial phase of the Templo Pintado [29].

The mean thicknesses of the individual layers are indicated in Fig. 4d–e.

Mineralogical composition (XRD)

The XRD patterns obtained from the analysis of the two surfaces and the plaster are shown in Fig. 5a, b and c.

The pale-yellow pigment samples revealed that the mineral responsible for the characteristic coloration is jarosite (Fig. 5a). Other identified phases include quartz, mica/illite group minerals, and plagioclases. In subordinate amounts, gypsum, amphibole group minerals, and chlorite group minerals were also detected. Quantitative analysis confirmed the presence of clay minerals belonging to the chlorite group in a weight percentage of approximately 2%. Additionally, a significant amount (about 13 wt%) of an illite-group clay mineral was clearly identified, indicating a non-negligible contribution of phyllosilicates to the pigment matrix. The identification of jarosite is consistent with most recent analytical studies carried out on different sectors of the North Front [29,45–47] and allows this phase to be related to the "lemon-yellow" pigment described by Muelle and Wells (1939), which they distinguished from yellow ochre pigments, for which limonite was instead identified [38]. In the broader Pachacamac context, jarosite is therefore interpreted as an intentionally selected pigment, since it is systematically reported as the main constituent of pale yellow paint layers and within pigment preparation tools [52].

The main mineral phases identified in the vermilion red pigment sample are quartz and plagioclases (Fig.5b). In subordinate amounts, gypsum, mica/illite group minerals, pyroxenes, and chlorite group minerals were also detected. Iron oxide in the form of hematite was clearly present and is responsible for the characteristic red coloration of the pigment. Quantitative analysis confirmed the presence of clay minerals belonging to both the chlorite and illite groups, with a combined weight percentage of approximately 14.5%, indicating a significant phyllosilicate component within the pigment matrix. These results are also in agreement with most previous studies carried out on different sectors of the North Front, confirming a consistent mineralogical signature for the vermilion red across the *Templo Pintado* [29,38,45–47] (see Supplementary

Information S1). A partial discrepancy is observed with the study by Faria et al. [44], in which hematite was detected by Raman spectroscopy but not by XRD and was therefore interpreted as poorly crystalline (see Supplementary Information S1). In contrast, in the present study and in recent investigations, the hematite phase is clearly resolved by XRD, indicating a well-crystallized iron oxide component in the red pigment.

Finally, the plaster layer is characterized by a mineralogical composition dominated by quartz and feldspars, including potassium feldspars and plagioclases (Fig. 5c). In subordinate amounts, mica/illite group minerals and chlorite group minerals were detected, together with minor contributions from amphibole- and pyroxene-group minerals, as well as trace amounts of smectite-group clays. Quantitative phase analysis confirmed that clay minerals belonging to the chlorite group account for approximately 4 wt% of the plaster composition, while mica/illite phases are present in minor proportions. While some previous studies characterized the clay component of the plaster primarily as illite [29,44], the present study is consistent with the investigations carried out in 2015 and in 2022-2023 in identifying, in addition to illite-group minerals, clay phases belonging to the chlorite and smectite groups [45–47] (see Supplementary Information S1). This mineralogical assemblage represents an essential diagnostic factor for understanding the physical degradation mechanisms affecting the *Templo Pintado* [46,47,53]. The observed differences in the results are consistent with the intrinsic nature of earthen materials, which can exhibit a high degree of compositional and granulometric heterogeneity.

Raman Spectroscopy

Raman spectroscopy was employed to identify the pigments and matrix components present in the painted fragments (Fig. 2) from the *Templo Pintado*.

The Raman spectra of the studied fragments are reported in Figure 6. The spectrum of the vermilion red surface fragment (TP_B) exhibits major bands at 153, 225, 283, 401, and 613 cm^{-1}, characteristic of hematite (α-Fe_2O_3), identified as the primary red pigment [54]. Additional bands at 573 and 693 cm^{-1} are assigned to silicate components, mainly quartz or feldspar, belonging to the plaster matrix, while those at 786 and 880 cm^{-1} correspond to carbonate vibrations (calcite and dolomite), suggesting a carbonate-silicate substrate.

A second spectrum was acquired from the underlying red stratum of the sample (Garnet Red). This measurement was performed on a stratigraphic layer naturally exposed along the fragment edge, as described in the Methods section. This analysis reveals additional bands at approximately 140 and 513 cm^{-1}. These low-frequency signals are not characteristic of hematite and are consistent with the Eg and A1g modes of anatase (TiO_2), typically found at ~144 cm^{-1} and ~513 cm^{-1} [55]. The detection of anatase (titanium dioxide) in the micro-stratigraphy of the *Templo Pintado* is directly supported by historical records of early 20th-century conservation efforts. Documentation from the 1938 intervention led by Albert A. Giesecke reveals that newly discovered mural paintings were treated with a variety of modern industrial materials to prevent deterioration [56,57]. Specifically, Giesecke reported the application of "liquid cement" (*cemento líquido*) over the polychrome designs of fish and birds. Historical correspondence also confirms the use of synthetic fixatives such as Ambroid, Alvar 770 (a polyvinyl acetal resin), and Valspar (a commercial varnish) [56,57]. These materials, common in the 1930s for "cleaning and consolidation", often contained titanium dioxide as an opacifier or stabilizer. The application method involving sprayers and brushes ensured that these exogenous compounds were intimately mixed with the original pigments. Furthermore, records indicate that conservation liquids were supplied for reapplication every three months, potentially increasing the concentration of these modern additives over time [29,56–58]. Consequently, the presence of anatase serves as a documented chemical marker of the 1938 restoration works rather than being part of the original pre-Hispanic palette.

The Raman spectrum of the yellow ochre layer, identified as the third layer within the stratigraphy of sample TP_B, shows characteristic bands corresponding to hematite (α-Fe_2O_3) and goethite (α-FeOOH) [59], indicating the main red and yellow pigments used. Additional peaks are assigned to carbonates (calcite/dolomite) and gypsum ($CaSO_4 \cdot 2H_2O$).

In the pale yellow part was detected the presence of illite, indicated by characteristic low-frequency vibrations around 439 cm^{-1}, consistent with tetrahedral Si-O-Al deformations [60].

Peaks in the 786-1103 cm^{-1} range are assigned to carbonates (calcite/dolomite) and silicate components, suggesting a carbonate-silicate substrate. The spectrum also shows features attributable to anatase (TiO_2), typically observed around 144, 197, 399, 513, and 639 cm^{-1}. Overall, the material consists of clay minerals, carbonate-silicate matrix, minor organic additives, and anatase.

The presence of a rising background and two broad bands between 1200 and 1700 cm^{-1} can be attributed to organic compounds, which may derive from residues of original binders, degradation products, or possibly other non-binder materials. The contribution of exogenous contaminants cannot be excluded. These features are not sufficient for an unambiguous identification of specific organic compounds; however, historical and ethnographic sources may provide contextual information useful for discussing potential interpretations of the observed signals. Within this context, the Raman data presented here provide suggestive, non-specific indications of organic constituents in the *Templo Pintado* paint layers. Pre-Hispanic painters commonly employed a variety of natural binding media, including plant gums, resinous substances from coniferous or tropical species, mucilaginous extracts derived from cactus or agave, and occasionally animal-derived products, such as egg or proteinaceous adhesives. These materials were often mixed with mineral pigments or applied as preparatory coatings to enhance paint adhesion [22].

From an analytical perspective, the Raman response is expected. Organic materials in archaeological contexts tend to undergo extensive alteration, polymerization, and oxidation, which diminish their Raman cross-sections and produce broad, featureless bands rather than sharp diagnostic peaks. Furthermore, the advanced state of degradation, likely involving polymerization and oxidation, leads to an amorphization of the spectral bands. In this context, the absence of FTIR and GC-MS analyses represents a methodological limitation of the study, as these complementary techniques could potentially provide additional information on organic functional groups. However, in the present samples, any spectroscopic contribution from such compounds is expected to be weak and partially obscured by the strong absorption and scattering effects of the inorganic matrix (silicates and carbonates), making their interpretation non-trivial. Overall, the Raman results indicate that the *Templo Pintado* polychromy is mainly based on iron oxide pigments (hematite and goethite), applied over a carbonate-silicate plaster containing clay minerals (illite). The detection of anatase (TiO_2) points to possible modern interventions or later contamination, while the weak organic signals between 1200 and 1700 cm^{-1} support the hypothesis of the use of natural organic binders of plant or resinous origin. These findings provide long-sought analytical support for hypotheses formulated since the early 20th century, which had remained unconfirmed in all subsequent investigations.

SEM-EDS

SEM-EDS analysis provides a compositional framework that closely aligns with the mineralogical information obtained from Raman spectroscopy, together offering a multi-analytical stratigraphic reconstruction based on representative samples and material heterogeneity (Fig. 7). The chemical data (see S10, S11, S12 and S13 in Supplementary Information) show a predominantly silicate-carbonate matrix in which iron-rich phases, clay components, and minor additional minerals are variably distributed. Several analysed points show significant Fe enrichment, most notably TP_B pale yellow with ~17 wt% Fe, and TP_B Red – 2nd layer_pt1(Garnet Red) and TP_B Red surface (Vermilion Red) with ~9-10 wt%, which is consistent with the Raman identification of hematite and goethite through their characteristic spectral bands. These correlations strongly support the presence of iron oxide pigments, likely responsible for reddish or ochre tonalities observed in the material. On the contrary, points with high Si and Al contents, particularly TP_B Red – 2nd layer_pt2 (Si ~29 wt%), reflect zones dominated by a silicate matrix composed of quartz, feldspars, and illitic clays, all of which are confirmed by Raman analysis. Calcium is present in generally low to moderate concentrations (0.5-2.7 wt%), and its heterogeneous distribution is compatible with s16tabilized carbonate phases such as calcite and dolomite detected by Raman. The notably elevated S content in TP_B yellow (~7 wt%) further reinforces the Raman evidence for gypsum ($CaSO_4 \cdot 2H_2O$), suggesting either the presence of a sulfate-rich component within the plaster or the accumulation of secondary sulfate crusts or microcrystalline deposits. The detection of Ti in trace amounts (e.g., TP_B Red – 2nd layer_pt1: ~0.35 wt%) corresponds to the Raman identification of anatase, which likely represents a minor phase introduced either through environmental contamination or more recent restoration materials.

Carbon concentrations vary widely, ranging from ~1 to >10 wt%. Although carbon concentrations (1-10 wt%) may be influenced by environmental adsorption or the intrinsic porosity of the earthen mortar, their detection within the inner layers exposed along the lateral edges of the fragment, and not just on the surface, suggests they are intrinsic to the original stratigraphy. This spatial distribution is crucial to distinguish these signals from modern contaminants, such as the synthetic fixatives associated with the 1938 restoration (marked by the presence of anatase), which were primarily applied to the outermost layers. This is further confirmed by Raman spectroscopy:

the broad, low-intensity features observed in the 1200-1700 cm^{-1} region support the hypothesis of the use of organic binders, coatings, or their degradation products. The identification of these organic components within the stratigraphic layers aligns with historical reports regarding the use of organic additives in the *Templo Pintado* [38]. Additional minor and trace elements detected, such as Ba, Na, Mg, and K, further support the presence of barite inclusions, clay minerals, and soluble salts commonly associated with historic plasters and alteration processes. Taken together, the combined SEM-EDS and Raman data describe a complex, multi-component material in which pigment particles, silicate aggregates, carbonate phases, and both ancient and possibly modern accessory minerals coexist, providing a better understanding of the material's composition, provenance, and state of preservation. The integration of SEM-EDS with Raman and XRD data establishes, for the first time, a coherent diagnostic framework capable of distinguishing ancient materials from later deposits or contaminants.

The integrated multi-analytical investigation carried out on painted plaster fragments from Sector 3 of the North Front of the Templo Pintado provides a coherent and robust diagnostic framework that significantly advances current knowledge on the materials, technology, and conservation state of this emblematic earthen mural system.

First, the mineralogical results confirm a clear technological continuity between Sector 3 and other previously studied areas of the monument. The pale yellow pigment is unequivocally associated with jarosite, while the so-called vermilion red is based on well-crystallized hematite. The plaster substrates consist of a silicate, carbonate matrix enriched in phyllosilicates, particularly illite and chlorite, together with subordinate quartz and feldspar phases. This mineralogical assemblage demonstrates a consistent technological palette across different sectors and pictorial phases, indicating a standardized selection of locally available raw materials and well-established preparation practices.

A second and particularly significant outcome of this study concerns the long-standing debate on the presence of organic binders in the painting technology. Weak but reproducible Raman signals in the 1200-1700 cm^{-1} spectral region, together with the detection of carbon within internal stratigraphic layers through SEM-EDS, may be consistent with the possible presence of organic components, although these observations are non-specific and do not allow an unambiguous

attribution, and alternative sources such as amorphous carbon, degradation products, or contamination cannot be excluded.

The analytical data therefore lend scientific support to the historical hypothesis formulated by Muelle and Wells (1939) regarding the use of plant-derived or resinous additives, resolving an issue that has remained unresolved for decades due to the intrinsic analytical challenges associated with degraded organic materials.

The study also allowed the identification of anatase (TiO_2) within the stratigraphy, which is thought to be associated with conservation work carried out in the early 20th century. Historical documentation suggests a correlation between this phase and the application of synthetic fixatives and liquid consolidants during the restoration campaigns of 1938. This result highlights the fundamental role of stratigraphic microanalysis in distinguishing original materials from those resulting from subsequent interventions or contaminations.

From a structural and degradation perspective, the analyses reveal a highly complex multi-layer stratigraphy, characterized by repeated episodes of repainting and maintenance over time. Distinct degradation behaviours were observed among the different pigment types: jarosite-based yellow surfaces exhibit pronounced chalking, likely related to weak cohesion and mineral instability, whereas hematite-rich red layers generally maintain greater cohesion but tend to exfoliate and flake. The presence of hygroscopic clay minerals and soluble sulfates, particularly gypsum, within the plaster matrix appears to play a key role in controlling deterioration mechanisms, as these phases promote moisture-induced swelling and progressive mechanical weakening.

Finally, the results provide essential baseline data for conservation planning. The identification of both mineralogical composition and residual organic components establishes a scientifically grounded framework for selecting compatible consolidants and treatment strategies. In particular, the hypothesized presence of organic binders requires careful evaluation of solvent-based interventions to avoid unintended dissolution or chemical alteration. Moreover, the diagnostic dataset offers a reference point for long-term monitoring of degradation processes in relation to environmental stressors.

In summary, this study demonstrates that the pictorial technology of the North Front of *Templo Pintado* is based on a sophisticated combination of iron-oxide and sulfate pigments applied over

clay-rich earthen plasters, supplemented by what appear to be organic additives, as suggested by convergent Raman and SEM-EDS evidence. By integrating stratigraphic, mineralogical, and microchemical evidence, the present work provides a scientific contribution to the interpretation of technological practices and supports future conservation strategies.

Acknowledgments

The authors acknowledge support from the University of Cagliari under Open Access funding call for the publication of this work. In addition, we sincerely thank the entire staff of the Museo Pachacamac for their support and collaboration. This research was funded by Fondazione di Sardegna, project FDS2022 “New diagnostic techniques for ancient books restauration and conservation” CUP F73C23001560007 and project FDS2023 “Preparation and characterization of biodegradable nanostructured carbon-based conductive pastes and inks” CUP F23C25000290007.

Availability of Data and Materials:

All the data generated during the present investigation are presented within the manuscript and Supplementary Information.

Conflict of interest

The authors declare no competing financial or non-financial interests.

Author Contributions

M.C. and S.P. conducted experiments, performed analysis and wrote the original manuscript. M.C., D.C., G.P., D.P.E., G.P.N. and S.P. edited, reviewed, and improved the manuscript. M.C. and S.P. did the final corrections in the manuscript. D.C. and G.P. reviewed and provided with funds and resources. D.C. and G.P. supervised and managed the project. All authors have critically reviewed and approved the final draft of the manuscript.

References

1. Blasco-López, F. J., Alejandre, F. J. & Flores-Alés, V. Methodology for characterising microlayers in historical plasterwork. *Constr. Build. Mater.* **93**, 463–470; 10.1016/j.conbuildmat.2015.05.135 (2015).
2. Carò, F. & Di Giulio, A. Reliability of textural analysis of ancient plasters and mortars through automated image analysis. *Mater. Charact.* **53**, 243–257; 10.1016/j.matchar.2004.06.014 (2004).
3. Ma, X. *et al.* Multi-analytical Studies of Archaeological Chinese Earthen Plasters: The Inner Wall of the Longhu Hall (Yuzhen Palace, Ancient Building Complex, Wudang Mountains, China). *Archaeometry* **60**, 1–18; 10.1111/arcm.12318 (2018).
4. Cappai, M., Casti, M. & Pia, G. Monitoring and preservation of stone cultural heritage using a fuzzy model for predicting salt crystallisation damage. *Sci. Rep.* **14**, 22671; 10.1038/s41598-024-73192-3 (2024).
5. He, J. *et al.* A multi-analytical approach for the characterization of materials, manufacturing process and damage mechanisms of wall paintings in Samye Temple, Tibet. *Dyes and Pigments* **207**, 110704; 10.1016/j.dyepig.2022.110704 (2022).
6. Dighe, B. B. & Singh, M. R. Promoting conservation sustainability: Analysing biomaterials in 6–8th century Aurangabad cave mud plasters. *J. Cult. Herit.* **74**, 276–288; 10.1016/j.culher.2025.06.020 (2025).
7. Wang, Y. & Wu, X. Current progress on murals: distribution, conservation and utilization. *Herit. Sci.* **11**, 61; 10.1186/s40494-023-00904-9 (2023).
8. Song, Y. *et al.* A technical study of the materials and manufacturing process used in the Gallery wall paintings from the Jokhang temple, Tibet. *Herit. Sci.* **6**, 18; 10.1186/s40494-018-0182-5 (2018).
9. Albert-Tortosa, F. *et al.* Environmental effects on surface lead–calcium apatite formation on Roman wall paintings. *Sci. Rep.* **15**, 18583; 10.1038/s41598-025-03620-5 (2025).
10. Zheng, L. *et al.* Blurring of ancient wall paintings caused by binder decay in the pigment layer. *Sci. Rep.* **10**, 21075; 10.1038/s41598-020-78117-4 (2020).
11. Shao, M., Li, L., Wang, S., Wang, E. & Li, Z. Deterioration mechanisms of building materials of Jiaohe ruins in China. *J. Cult. Herit.* **14**, 38–44; 10.1016/j.culher.2012.03.006 (2013).
12. Singh, M. & Arbad, B. R. Characterization of 4th–5th century A.D. earthen plaster support layers of Ajanta mural paintings. *Constr. Build. Mater.* **82**, 142–154; 10.1016/j.conbuildmat.2014.04.126 (2015).
13. Ma, X. Deterioration of Earthen Building Materials. in *The Encyclopedia of Archaeological Sciences* 1–4; 10.1002/9781119188230.saseas0171 (Wiley, 2018).
14. Ogura, D. *et al.* Influence of Environmental Factors on Deterioration of Mural Paintings in Mogao Cave 285, Dunhuang. in *Case Studies in Building Rehabilitation. Building Pathology and Rehabilitation* (ed. Delgado, J. M. P. Q.) 105–159; 10.1007/978-3-030-49202-1_6 (2021).
15. Cappai, M. & Pia, G. Sustainable clay-based materials stabilised by low-temperature treatments: Salt degradation and chemomechanical approach. *Results in Engineering* **27**, 106222; 10.1016/j.rineng.2025.106222 (2025).

16. Singh, M. R., Ragde, R., Baroi, S. & Banerjee, D. Unravelling the composition and provenance of mud plasters in the Aurangabad Caves: a multifaceted analytical approach. *Discov. Mater.* **5**, 208; 10.1007/s43939-025-00281-z (2025).
17. Anand, P., Balaji, A. & Mani, M. A multi-analytical investigation of inorganic pigments' composition in Kerala mural and Theyyam folk art. *npj Heritage Science* **14**, 192; 10.1038/s40494-026-02453-3 (2026).
18. Gebremariam, K. F., Kvittingen, L. & Nicholson, D. G. Multi-analytical investigation into painting materials and techniques: the wall paintings of Abuna Yemata Guh church. *Herit. Sci.* **4**, 32; 10.1186/s40494-016-0101-6 (2016).
19. Liu, W. *et al.* Multi-Analytical Approach to Investigate the Polychrome Paintings on Flower Peking Opera Theatre in Bozhou, China. *Coatings* **16**, 115; 10.3390/coatings16010115 (2026).
20. Gong, Y. *et al.* A multi-analytical investigation of different gilding techniques in the mural painting of the Yuan Dynasty (A.D. 1271-1368). *npj Heritage Science* **13**, 514; 10.1038/s40494-025-02091-1 (2025).
21. Gong, Y. *et al.* Multianalytical Studies on the Mural Painting of Yongle Palace in Shanxi Province, China. *Archaeometry* **68**, 36–47; 10.1111/arcm.70025 (2026).
22. Guasch-Ferré, N., Pérez, J. L. P., Pascual, M. L. V. de Á., Osete-Cortina, L. & Doménech-Carbó, M. T. Polysaccharide remains in Maya mural paintings: is it an evidence of the use of plant gums as binding medium of pigments and additive in the mortar? *Sci. Technol. Archaeol. Res.* **5**, 200–220; 10.1080/20548923.2020.1720377 (2019).
23. Zheng, J. Choice of Materials for the Conservation of Wall Paintings on Earthen Supports in China. in *The Conservation of Decorated Surfaces on Earthen Architecture* (eds. Rainer, L. & Bass Rivera, A.) 99–109 (Getty Publication, Los Angeles, 2006).
24. Shekede, L. & Rickerby, S. Theory into Practice: Establishing Compatibility in Earth-Based Repair Materials. in *The Conservation of Decorated Surfaces on Earthen Architecture* (eds. Rainer, L. & Bass Rivera, A.) 89–98 (Getty Publication, Los Angeles, 2006).
25. Cappai, M. *et al.* Thermal Properties of Eco-Friendly Earthen Materials Stabilized with Bio-Based Polymers: Experimental Data and Modeling Procedure for Improving Mix-Design. *Materials* **17**, 1035; 10.3390/ma17051035 (2024).
26. Cuní, J. What do we know of Roman wall painting technique? Potential confounding factors in ancient paint media analysis. *Herit. Sci.* **4**, 44; 10.1186/s40494-016-0111-4 (2016).
27. Rivas, T., Pozo-Antonio, J. S., Jiménez-Desmond, D., Dionísio, A. & Cardell, C. Deterioration of White Tempera Mock-Ups Paints in a SO2-Rich Atmosphere. *Applied Sciences* **15**, 1610; 10.3390/app15031610 (2025).
28. Bass Rivera, A., Rainer, L. & Vagts, L. Out of Their Native Earth: The History of Excavation and Conservation of Ancient Hopi Murals from Awatovi and Kawaika-a. in *The Conservation of Decorated Surfaces on Earthen Architecture* (eds. Rainer, L. & Bass Rivera, A.) 53–65 (Getty Publication, Los Angeles, 2006).
29. Pozzi-Escot, D., Pacheco, G. & Uceda, C. R. *Pachacamac: Templo Pintado - Conservación e Investigación*. (Ministerio De Cultura, Lima, 2013).
30. Kottek, M., Grieser, J., Beck, C., Rudolf, B. & Rubel, F. World map of the Köppen-Geiger climate classification updated. *Meteorologische Zeitschrift* **15**, 259–263; 10.1127/0941-2948/2006/0130 (2006).

31. Peel, M. C., Finlayson, B. L. & McMahon, T. A. Updated world map of the Köppen-Geiger climate classification. *Hydrol. Earth Syst. Sci.* **11**, 1633–1644; 10.5194/hess-11-1633-2007 (2007).
32. Beck, H. E. *et al.* Present and future köppen-geiger climate classification maps at 1-km resolution. *Sci. Data* **5**, 1–12; 10.1038/sdata.2018.214 (2018).
33. Eeckhout, P. Change and permanency on the coast of ancient Peru: The religious site of Pachacamac. *World Archaeol.* **45**, 137–160; 10.1080/00438243.2012.759516 (2013).
34. Giraldo, J. A. R. *Santuario de Pachacámac: Cien Años de Arqueología En La Costa Central*. (Cultura Andina S.A.C., Lima, 2011).
35. Sepúlveda, M. *et al.* Unraveling the polychromy and antiquity of the Pachacamac Idol, Pacific coast, Peru. *PLoS One* **15**, e0226244; 10.1371/journal.pone.0226244 (2020).
36. Vega, G. D. La. *Comentarios Reales. Origen e Historia de Los Incas Del Peru (1609)*. (1970).
37. Pozzi-Escot, D. *et al.* Traces in the desert: use of new technologies for the study and valorization of the Pachacamac sanctuary—Lima, Peru. *Herit. Sci.* **6**, 68; 10.1186/s40494-018-0230-1 (2018).
38. Muelle, J. C. & Wells, R. Las pinturas del Templo de Pachacamac. *Revista del Museo Nacional* **8**, 265–282 (1939).
39. Pozzi-Escot, D. *Pachacamac: Conservación En Arquitectura de Tierra*. (Ministerio de Cultura, 2014).
40. Faria, D. L. A., Pacheco, G., Pozzi-Escot, D., Maier, M. S. & Careaga, V. Pigments from Templo Pintado (Pachacamac, Perú) investigated by Raman Microscopy. in *Book of Abstracts 7th International Congress on the Application of Raman Spectroscopy in Art and Archaeology (RAA 2013), 2th–6th September 2013* (Institute for the Protection of Cultural Heritage of Slovenia, Ljubljana, 2013).
41. Serra, J. C. *Análisis Cromático Del Templo Pintado de Pachacamac*. https://pachacamac.cultura.pe/investigaciones/templo-pintado (2015).
42. Cappai, M. *et al.* Degradation phenomena of Templo Pintado painted plasters. *Constr. Build. Mater.* **392**, 131839; 10.1016/j.conbuildmat.2023.131839 (2023).
43. Cappai, M. *et al.* Weathering of earth-painted surfaces : Environmental monitoring and artificial aging. *Constr. Build. Mater.* **344**, 128193; 10.1016/j.conbuildmat.2022.128193 (2022).
44. Bass, A. *et al.* Characterization and Comparative Analysis of Ancient Earthen Plasters from the American Southwest. *MRS Adv.* **2**, 2145–2178; 10.1557/adv.2017.240 (2017).
45. Zanchetta, L. M. *et al.* Microstructures of Building Materials from Huaca De La Luna, Peru. *International Journal of Architectural Heritage* **14**, 256–273; 10.1080/15583058.2018.1531181 (2020).
46. Jia, Q., Chen, W., Tong, Y. & Guo, Q. Laboratory study on shrinkage and cracking behavior of historic earthen plaster. *Eng. Geol.* **318**, 107096; 10.1016/j.enggeo.2023.107096 (2023).
47. Uhle, M. *Pachacamac. Report of the William Pepper M.D., LL.D. Peruvian Expedition of 1896*. (University of Pennsylvania Press, Philadelphia, PA, USA, 1903).
48. Bonavia, D. *Mural Painting in Ancient Peru*. (Indiana University Press, Bloomington, 1985).
49. Marcone Flores, G. Los murales del Templo Pintado o Relación entre el Santuario de Pachacamac y la iconografía tardía de la Costa Central Peruana. *Anales del Museo de América* **11**, 57–80 (2003).
50. Wright, V. Pigmentos y tecnología artística mochicas: una nueva aproximación en la comprensión de la organización social. *Bulletin de l'Institut français d'études andines* **39 (2)**, 299–330 ; 10.4000/bifea.1950 (2010).

51. Colonna-Preti, K., Eeckhout, P. & Luján Dávila, M. R. Pinturas y pintores en Pachacamac: un estudio multidisciplinario del Edificio B15. *Boletín de Arqueología PUCP* 9–31; 10.18800/boletindearqueologiapucp.201901.001 (2019).
52. Müller-Vonmoos, M. & Løken, T. The shearing behaviour of clays. *Appl. Clay Sci.* **4**, 125–141; 10.1016/0169-1317(89)90004-5 (1989).
53. Basavegowda, N., Mishra, K. & Lee, Y. R. Synthesis, characterization, and catalytic applications of hematite (α -Fe $_2$ O $_3$) nanoparticles as reusable nanocatalyst. *Advances in Natural Sciences: Nanoscience and Nanotechnology* **8**, 025017; 10.1088/2043-6254/aa6885 (2017).
54. Sekiya, T., Ohta, S., Kamei, S., Hanakawa, M. & Kurita, S. Raman spectroscopy and phase transition of anatase TiO2 under high pressure. *Journal of Physics and Chemistry of Solids* **62**, 717–721; 10.1016/S0022-3697(00)00229-8 (2001).
55. Asencios Lindo, R. G. Albert A. Giesecke Parthymüeller y la conservación en el Templo Pintado: documentos inéditos en torno de la conservación en Pachacamac en 1938. *Intervención, Revista Internacional de Conservación, Restauración y Museología* **10**, 36–50; 10.30763/Intervencion.2019.19.207 (2019).
56. Giesecke, A. *Archivo Albert Giesecke-Documentos (Folder: AGD- 194; AG-D-195; AG-D-0221; AG-D-1261)*. (1938).
57. Rubio Correa, M. A. *ALBERT ANTHONY GIESECKE PARTHYMUELLER 'El Más Peruano de Los Norteamericanos'*. (Nova Print, Lima, 2007).
58. Yandrisevits, M. A., Londero, P., Carò, F., Rizzo, A. & Cappuccini, C. Wavelength-dependent absorption and scattering effects on laser cleaning of a corroded iron alloy European scale armor. in *Proceedings of the International Conference LACONA XI* 27–45; 10.12775/3875-4.02 (Nicolaus Copernicus University Press, 2017).
59. Moncada, D. & Bodnar, R. Gangue mineral textures and fluid inclusion characteristics of the Santa Margarita Vein in the Guanajuato Mining District, Mexico. *Open Geosciences* **4**, 300–309; 10.2478/s13533-011-0057-8 (2012).

Figure captions

Fig. 1. (a) Satellite view of the Peruvian coast showing the location of Pachacamac (Google Earth Pro, Image © Google, Maxar Technologies); (b) satellite view of the Templo Pintado area with indication of the study zone (Google Earth Pro, Image © Google, Maxar Technologies): (c) view of the *Templo Pintado* in 2008, before the installation of the protective roof and the conservation works (Image courtesy of the Santuario Arqueológico de Pachacamac).

Fig. 2. (a) Plan of the Templo Pintado. The North Front is highlighted in red, while the yellow area indicates the sector from which the samples were collected during the removal and cleaning of collapse deposits (adapted and modified from Pozzi-Escot et al., 2013 [29]). (b–e) Sample TP_6: (b) surface before pigment removal; (c) surface after removal of the pale yellow superficial layer and exposure of the yellow ochre pigment; (d) lateral view; (e) schematic representation of the stratigraphy. The pale yellow surface layer was carefully removed using a steel scalpel to allow the collection of powder samples for mineralogical characterization by XRD. (f–h) Sample TP_B: (f) surface view and (g) lateral view; (h) schematic representation of the stratigraphy.

Fig. 3. Surface details of pale yellow painted sample TP_6 showing pigment powdering and irregular morphology (a), and exposure of an underlying yellow ochre layer with visible fibers (b).

Fig. 4. Detail of the surface of vermilion red sample TP_A showing: (a) brushstroke marks indicating pigment application technique; (b) pigment grain size and the presence of fine sand particles deliberately added during application; (c) cross-section of TP_C sample; (d) detail of the inner paint layers of TP_C sample; (e) detail of the superficial paint layers of sample TP_C.

Fig. 5. XRD patterns obtained from the analysis of: (a) pale yellow surface of sample TP_6; (b) vermilion red surface of sample TP_A; (c) plaster of sample TP_D. Grey line: experimental data; red line: calculated profile.

Fig. 6. Raman spectra of the stratigraphic layers of sample TP_B.

Fig. 7. SEM micrographs of TP_B fragments acquired at 20 kV in low-vacuum mode: (a) compact morphology of the vermilion red surface; (b) the second red layer (Garnet red) showing a silicate matrix; (c) the pale yellow layer exhibiting significant enrichment in iron and sulfur.

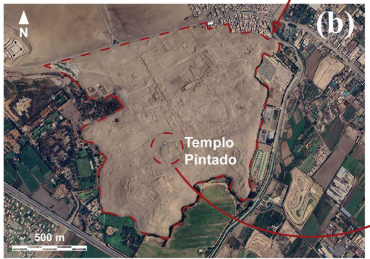

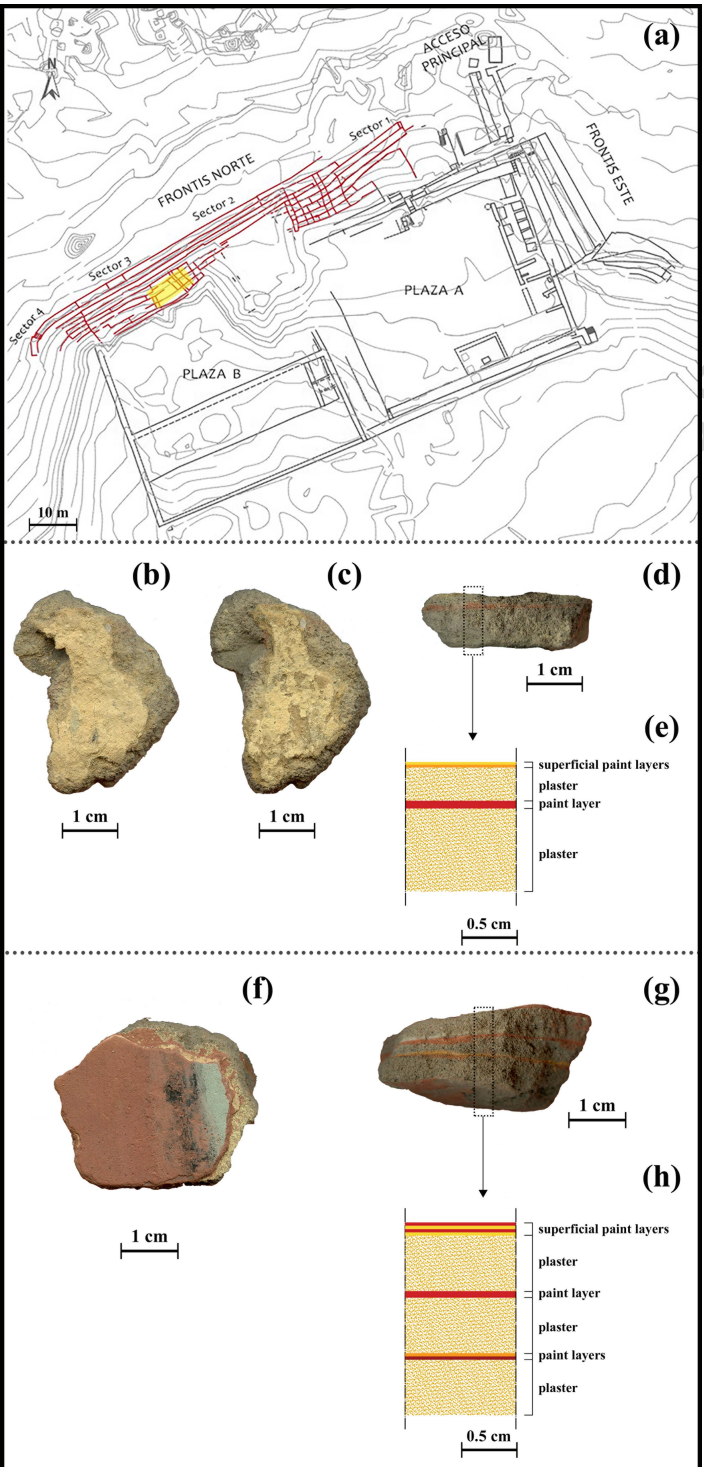
(a)
N
ACCESO PRINCIPAL
FRONTIS NORTE
FRONTIS ESTE
Sector 1
Sector 2
Sector 3
Sector 4
PLAZA A
PLAZA B
10 m
(b)
1 cm
(c)
1 cm
(d)
1 cm
(e)
superficial paint layers
plaster
paint layer
plaster
0.5 cm
(f)
1 cm
(g)
1 cm
(h)
superficial paint layers
plaster
paint layer
plaster
paint layers
plaster
0.5 cm

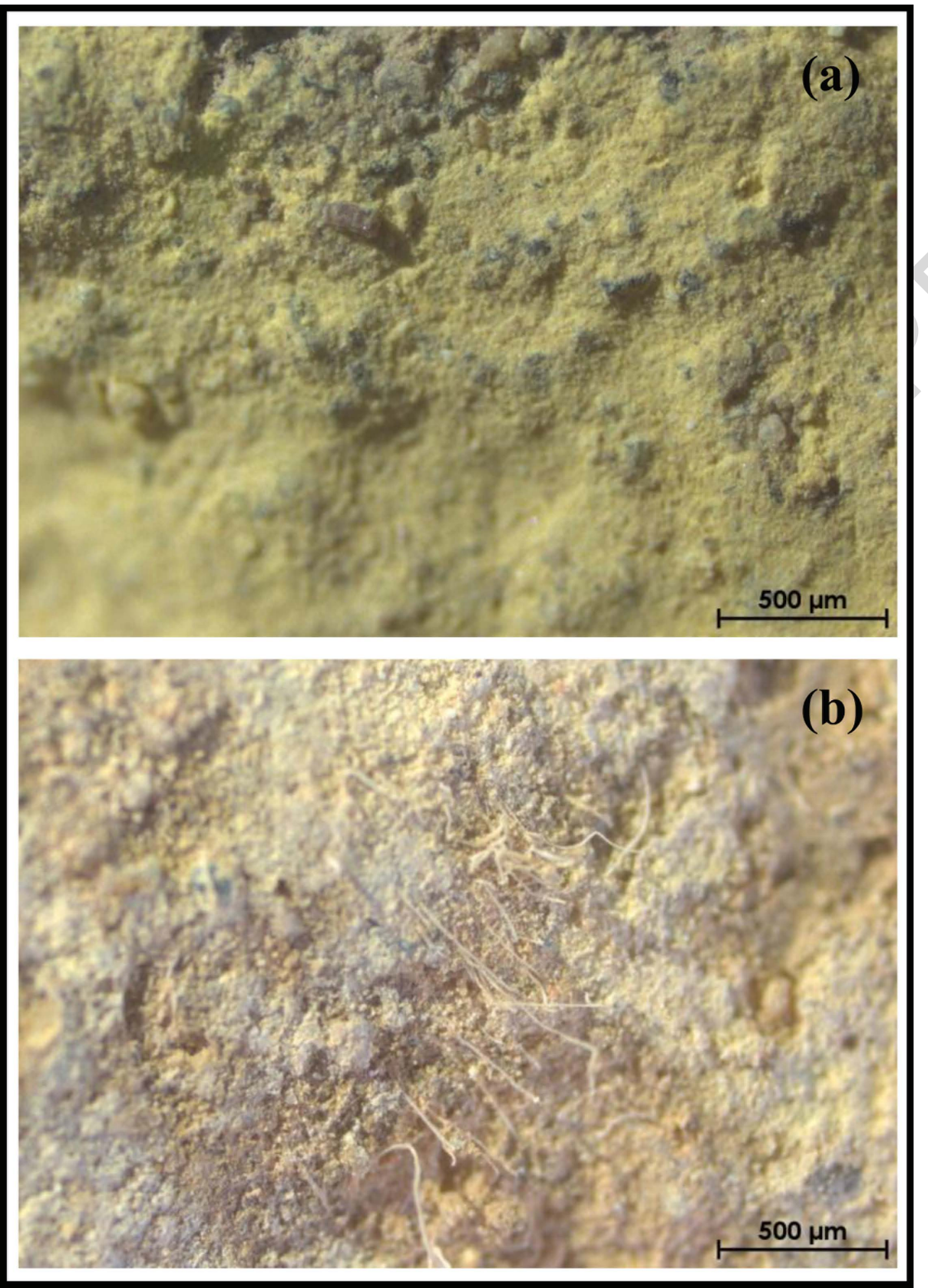

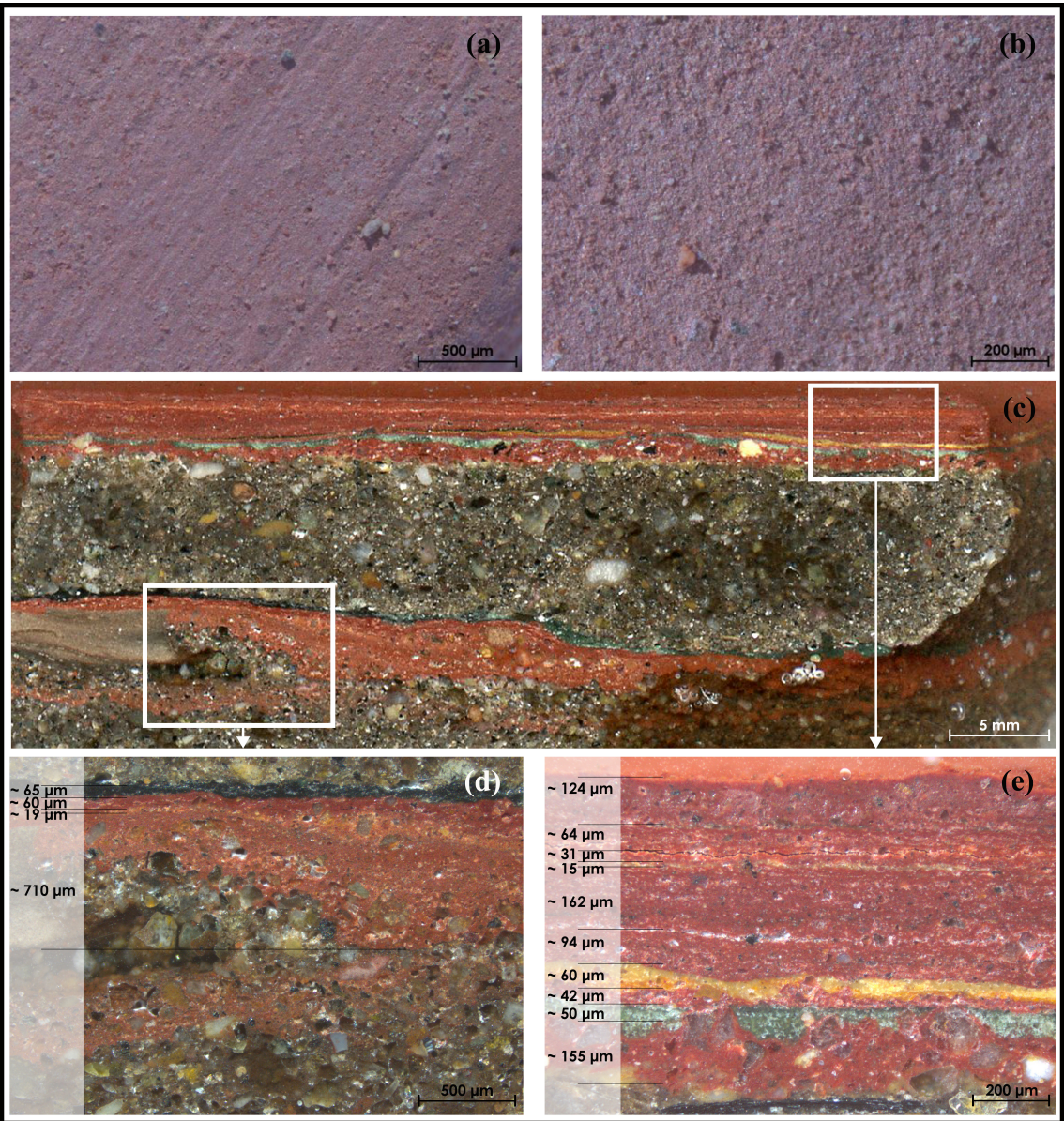
(a)
500 µm
(b)
200 µm
(c)
5 mm
(d)
~ 65 µm
~ 60 µm
~ 19 µm
~ 710 µm
500 µm
(e)
~ 124 µm
~ 64 µm
~ 31 µm
~ 15 µm
~ 162 µm
~ 94 µm
~ 60 µm
~ 42 µm
~ 50 µm
~ 155 µm
200 µm

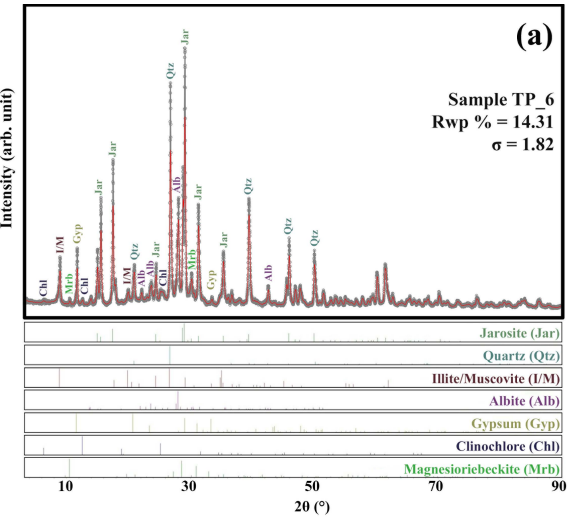

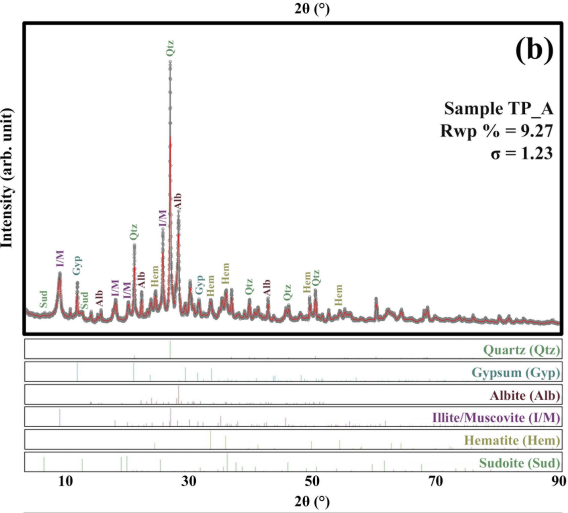

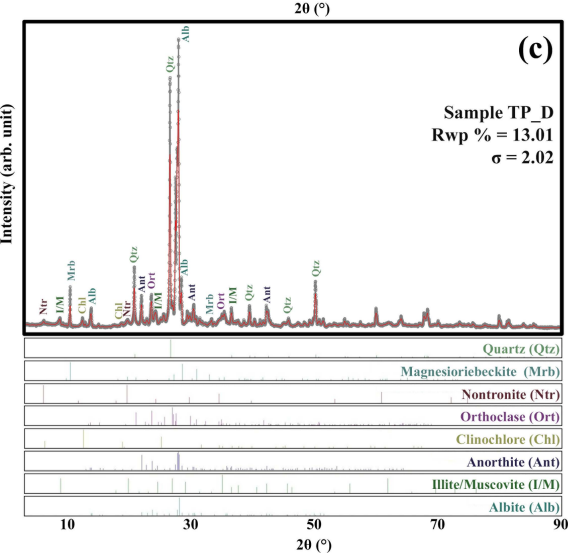

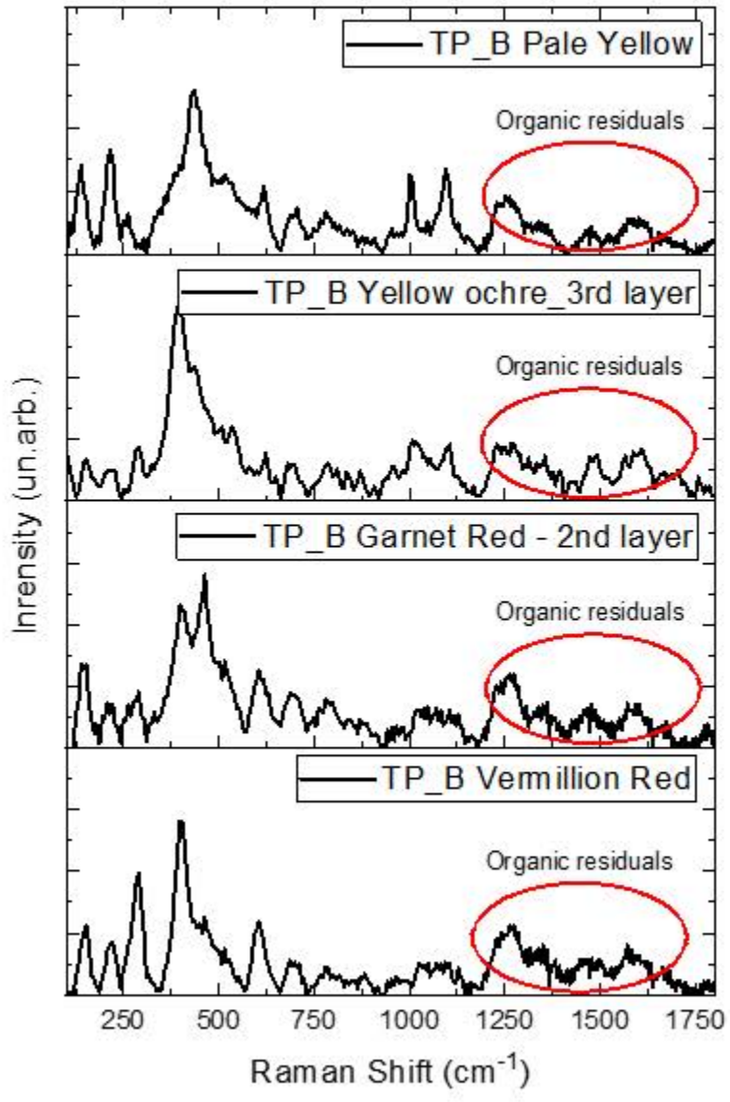
TP_B Pale Yellow
Organic residuals
TP_B Yellow ochre_3rd layer
Organic residuals
TP_B Garnet Red - 2nd layer
Organic residuals
TP_B Vermillion Red
Organic residuals
Inrensity (un.arb.)
250
500
750
1000
1250
1500
1750
Raman Shift (cm-1)

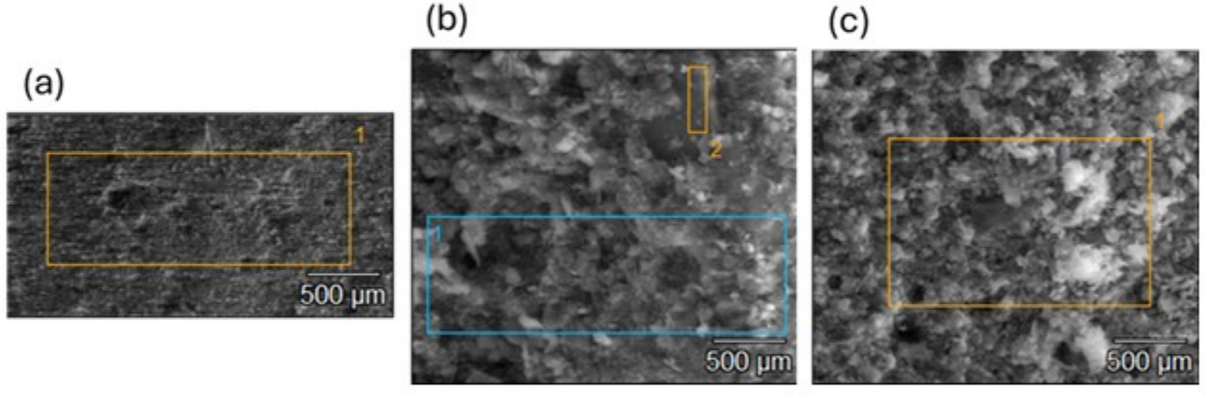
(a)
1
500 µm
(b)
2
1
500 µm
(c)
1
500 µm